

See discussions, stats, and author profiles for this publication at: <https://www.researchgate.net/publication/317276656>

Carbon-MEMS-Based Alternating Stacked MoS₂ at rGO-CNT Micro-Supercapacitor with High Capacitance and Energy...

Article in *Small* · May 2017

DOI: 10.1002/sml.201700639

CITATION

1

READS

48

9 authors, including:



Xiaocong Tian

Nanyang Technological University

30 PUBLICATIONS 877 CITATIONS

SEE PROFILE



Mengyu Yan

Seattle Children's Hospital

72 PUBLICATIONS 1,443 CITATIONS

SEE PROFILE



Jiashen Meng

Wuhan University of Technology

26 PUBLICATIONS 321 CITATIONS

SEE PROFILE



Liqiang Mai

Wuhan University of Technology

199 PUBLICATIONS 4,964 CITATIONS

SEE PROFILE

Some of the authors of this publication are also working on these related projects:



nanomaterials for energy storage [View project](#)



Emerging Prototype Sodium-Ion Full Cells with Nanostructured Electrode Materials [View project](#)

Carbon-MEMS-Based Alternating Stacked MoS₂@rGO-CNT Micro-Supercapacitor with High Capacitance and Energy Density

Wei Yang, Liang He,* Xiacong Tian, Mengyu Yan, Hui Yuan, Xiaobin Liao, Jiashen Meng, Zhimeng Hao, and Liqiang Mai*

A novel process to fabricate a carbon-microelectromechanical-system-based alternating stacked MoS₂@rGO-carbon-nanotube (CNT) micro-supercapacitor (MSC) is reported. The MSC is fabricated by successively repeated spin-coating of MoS₂@rGO/photoresist and CNT/photoresist composites twice, followed by photoetching, developing, and pyrolysis. MoS₂@rGO and CNTs are embedded in the carbon microelectrodes, which cooperatively enhance the performance of the MSC. The fabricated MSC exhibits a high areal capacitance of 13.7 mF cm⁻² and an energy density of 1.9 μWh cm⁻² (5.6 mWh cm⁻³), which exceed many reported carbon- and MoS₂-based MSCs. The MSC also retains 68% of capacitance at a current density of 2 mA cm⁻² (5.9 A cm⁻³) and an outstanding cycling performance (96.6% after 10 000 cycles, at a scan rate of 1 V s⁻¹). Compared with other MSCs, the MSC in this study is fabricated by a low-cost and facile process, and it achieves an excellent and stable electrochemical performance. This approach could be highly promising for applications in integration of micro/nanostructures into microdevices/systems.

1. Introduction

In past decades, electronic microdevices have been greatly developed, profiting from the tremendous decrease of their


spatial scale. Microscale energy storage devices, as an important component in microdevices/systems, are attracting increasing attention, accompanying the development of portable electronic products, wireless sensor networks, and integrated microsystems.^[1] As one kind of energy storage microdevices, micro-supercapacitors (MSCs) have a series of advantages, such as high power density, long lifetime, and environmental friendliness.^[2] There are two energy storage mechanisms in MSCs: electrical double layer capacitance (EDLC) and pseudocapacitance. The EDLC is mainly contributed from pure electrostatic charge that accumulated at the electrode/electrolyte interface. The pseudocapacitive MSC can achieve high capacitance by a rapid and reversible faradic reaction on the surface/subsurface of electrode materials.^[3] The capacitance of MSCs is highly dependent on the surface area of the active material that is accessible to the electrolyte ions.^[4] One effective strategy to improve the performance of MSCs is to realize high areal and volumetric utilization of the electrode materials.^[5]

As a typical 2D transition metal dichalcogenide, molybdenum disulfide (MoS₂) can potentially store charge by inter-sheet and intrasheet double layers over an individual atomic layer. The central Mo atoms possess a range of oxidation

W. Yang, Prof. L. He, Dr. X. C. Tian, Dr. M. Y. Yan, H. Yuan, X. B. Liao, J. S. Meng, Z. M. Hao, Prof. L. Q. Mai
State Key Laboratory of Advanced Technology for Materials Synthesis and Processing
Wuhan University of Technology
Wuhan 430070, P. R. China
E-mail: hel@whut.edu.cn; mlq518@whut.edu.cn



Dr. L. Q. Mai
Department of Chemistry
University of California
Berkeley, CA 94720, USA
Prof. L. He
Department of Materials Science and NanoEngineering
Rice University
Houston, TX 77005, USA

 The ORCID identification number(s) for the author(s) of this article can be found under <https://doi.org/10.1002/sml.201700639>.

DOI: 10.1002/sml.201700639

states from +2 to +6, displaying a typical pseudocapacitive behavior and delivering a high theoretical capacitance of $\approx 1000 \text{ F g}^{-1}$.^[6–10] However, the aggregation and poor electrical conductivity among atomic layers of MoS_2 hinder its large-scale applications in MSCs. Moreover, the facile microfabrication processes for effective integration of MoS_2 and its composites into MSCs are still lacking. Therefore, developing facile microfabrication of MoS_2 -composite-based MSCs is a critical challenge for their applications in microdevices/systems.^[11,12]

Photoresist-derived carbon is another extensively employed electrode material in MSC, which is pyrolyzed from various photoresists,^[13,14] due to its ultrafine micro/nanopatterning and easy microfabrication for different aspect ratios. The carbon microelectromechanical system (MEMS) is a unique platform for photoresist-derived carbon-based microdevices/systems, and the microfabrication of carbon-MEMS is fully compatible with current microtechnologies.^[15] Meanwhile, as a typical carbon material, photoresist-derived carbon has some outstanding properties, such as relatively low cost, a wide potential window, and chemical inertness.^[4,16,17] Recently, our group developed an optimized microfabrication process of pyrolyzed-carbon/chitosan-coated carbon-nanotube (CNT)-composite microelectrodes-based MSC. The fabricated MSC delivered a high areal capacitance of 6.09 mF cm^{-2} (energy density of 4.5 mWh cm^{-3}) and an enhanced capacitance retention rate, attributing to the outstanding electrical conductivity and relatively high capacitance of CNT.^[18] However, the heteroatoms in photoresist are evaporated until only carbon with low specific surface area (SSA) remains, leading to significant weight loss and volume shrinkage of photoresist during pyrolysis. These results sometimes pose negative effects on the pyrolyzed carbon microelectrodes.^[1,17]

Herein, we propose a facile approach to fabricate photoresist-derived carbon-based all-solid-state MSCs. The microelectrodes are embedded with MoS_2 @reduced-graphene-oxide (rGO) and multiwalled CNTs (MWCNTs), which synergistically enhance the performance of MSCs. The

fabricated MSC shows a high areal capacitance, good capacitance retention rate, high energy density, and outstanding cycling performance. In the construction of MSCs, MoS_2 @rGO/photoresist (M-photoresist) and MWCNT/photoresist (C-photoresist) composites are prepared. The alternating stacked film is achieved by repeated spin coating of C-photoresist and M-photoresist for twice (denoted as MCMC-film). Then the interdigital micropatterns are fabricated by optimized photolithography, developing, and rinse. After pyrolysis and coating of H_2SO_4 /polyvinyl-alcohol (PVA) gel electrolyte, the MCMC-MSC is completely assembled. Benefiting from the alternating stacked structures, MCMC-MSC exhibits a high areal capacitance of 13.7 mF cm^{-2} and an energy density of 5.6 mWh cm^{-3} (0.1 mA cm^{-2}), exceeding those of most reported MoS_2 and photoresist-derived carbon-based MSCs. In addition, the fabricated MSC reveals an excellent capacitance retention of 68% from 0.1 to 2 mA cm^{-2} (0.3 to 5.9 A cm^{-3}) and a remarkable cycling performance over 96% after 10 000 cycles (1 V s^{-1}).

2. Results and Discussion

To obtain the detailed information of phase and morphology evolution for M-photoresist after annealing, the X-ray diffraction (XRD), scanning electron microscopy (SEM), transmission electron microscopy (TEM), and high resolution TEM (HRTEM) characterizations were performed. The EM image shows that the thin MoS_2 nanosheets@rGO are synthesized by a conventional one-step hydrothermal method (H- MoS_2) (Figure 1a).^[19] M-photoresist was annealed at 900°C in N_2 flow, and the MoS_2 @rGO/carbon composite was achieved (C- MoS_2). MoS_2 nanosheets@rGO are also reserved well in the C- MoS_2 composite (Figure 1b). As a control sample, H- MoS_2 was annealed at 900°C in N_2 flow and the MoS_2 nanosheets@rGO are well reserved (A- MoS_2) (Figure S1a, Supporting Information). MoS_2 nanosheets have higher SSA compared with the bulk MoS_2 and restacked exfoliated- MoS_2 nanosheets, providing a larger number of

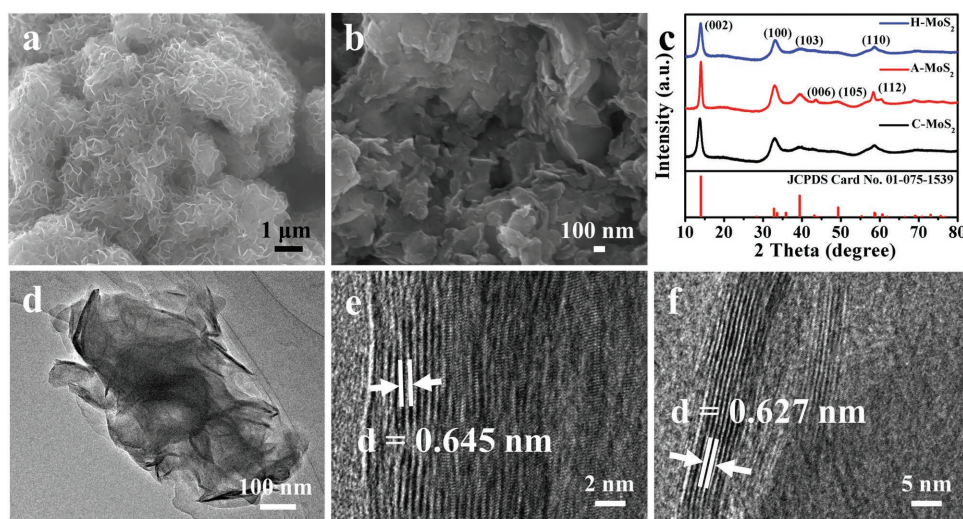


Figure 1. Characterization results of the samples. SEM images of a) H- MoS_2 and b) C- MoS_2 . c) XRD patterns of the three samples (H- MoS_2 , A- MoS_2 , and C- MoS_2). d) TEM image of H- MoS_2 . HRTEM images of e) H- MoS_2 and f) C- MoS_2 .

active sites for fast and reversible surface redox reactions.^[12] Figure 1c shows the XRD patterns of H-MoS₂, A-MoS₂, and C-MoS₂. For H-MoS₂, three sharp peaks at 13.7° (002), 32.9° (100), and 58.7° (110), and a low sharp peak at 39.5° (103) are observed. The excursion of (002) peak is probably caused by the intercalation of reaction ions in the layers during the hydrothermal process.^[20,21] For A-MoS₂, a sharp (002) peak appears at 14° that results from de-intercalation of the ions during high-temperature annealing. (103) peak becomes sharper; three low sharp peaks at 43.4° (006), 49.4° (105), and 60.3° (112) are observed. Simultaneously, narrow (002) and (110) peaks can be observed, which could be caused by the crystal growth, and all of the peaks are indexed to the hexagonal phase of MoS₂ (JCPDS Card No. 01-075-1539). For C-MoS₂, the (002), (100), (103), and (110) peaks can be assigned to hexagonal MoS₂ without narrowing. The photoresist separates the MoS₂ nanosheets, impedes the mass transfer of MoS₂, and retards their crystal growth. Therefore, the compositing with photoresist would inhibit the crystal growth of the MoS₂ without reaction.

Figure 1d–f demonstrates the representative TEM and HRTEM images of H-MoS₂ and C-MoS₂. As shown

in Figure 1d, H-MoS₂ shows the typical morphology of nanosheets, which is consistent with the SEM images, indicating that the MoS₂ layers are not stacked together. Figure 1e reveals that the H-MoS₂ is composed of tightly stacked structures. The HRTEM image of H-MoS₂ shows an interlayer distance of 0.645 nm, which is consistent with the result calculated from XRD pattern. As shown in Figure S1b (Supporting Information), the selected-area electron diffraction (SAED) pattern demonstrates that the H-MoS₂ has a similar crystalline structure as reported in previous work.^[22] Figure S1c (Supporting Information) shows the HRTEM image of A-MoS₂, the interlayer distance of 0.624 nm is in agreement with the calculation result obtained from XRD pattern, and the SAED (Figure S1d, Supporting Information) of the A-MoS₂ can also confirm this interlayer distance. The HRTEM image (Figure 1f) of the C-MoS₂ indicates that the interlayer spacing is about 0.627 nm. It demonstrates that the interlayer spacing decreases after annealing, which would lead to a stabilized crystal structure of 2H-MoS₂.

The microfabrication process of the MCMC-MSC is shown in **Figure 2a**. First, M-photoresist and C-photoresist composites are prepared. MCMC-film is achieved by

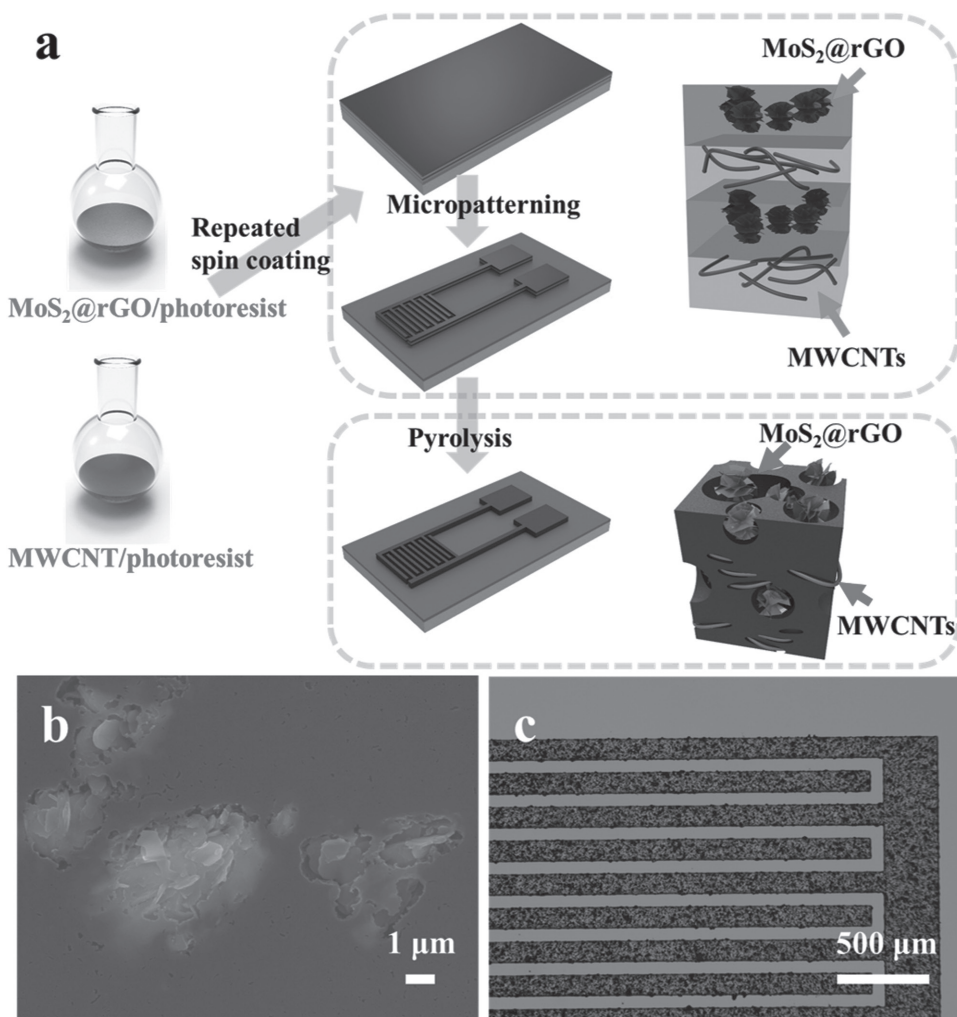


Figure 2. Microfabrication process and SEM image of stacked MSCs. a) The schematic of microfabrication process of MCMC-MSC. b) SEM image of MCMC-MSCs surface. c) The optical microscopic image of microelectrodes.

repeated spin coating of the MC-film (M-photoresist is spin coated on the C-photoresist) for twice. Then the interdigital micropatterns are fabricated by optimized photolithography, developing, and rinse. During the pyrolysis process, photoresist shrinks drastically,^[23] leading to partial interface separation between MoS₂@rGO and carbon, which is also observed at the interface between MWCNT and carbon (Figure S2, Supporting Information). In the MoS₂@rGO/carbon layer (M-layer), MoS₂ nanosheets are embedded in the carbon with gaps around their interfaces. Figure 2b exhibits the SEM image of the surface of the microelectrode; the gaps are intensively distributed around MoS₂ nanosheets, with a large surface exposed, and can be offered for contacting with the electrolyte. As Figure 2c shows, the MCMC-MSC exhibits a morphology of intact microelectrodes with a fine pattern and dense distribution of active materials. Cross-sectional SEM-energy-dispersive-spectroscopy mappings were conducted to characterize the stacked microelectrodes. As shown in Figure S3 (Supporting Information), the layered distribution of elements C, Mo, and S is realized, which is in agreement with the stacked structures.

The electrochemical performance of all-solid-state MCMC-MSC with an average thickness of 3.4 μm was studied by two-electrode cyclic voltammetry (CV) and galvanostatic charge/discharge (GCD) measurements. Also, the electrochemical performance of C-MSC, M-MSC, MC-MSC, and MCM-MSC was characterized for comparison with MCMC-MSC by a similar microfabrication process. In addition, to investigate the function of MWCNT, a blank control sample was also fabricated by stacking of photoresist and M-photoresist, following the same process as MCMC-MSC, denoted as MPMP-MSC (Figure S4, Supporting Information). Figure 3a–c exhibits the comparison of CV curves of

stacked MSCs. At a low scan rate, it is known that a rectangular CV curve would indicate the pure EDLC;^[24] however, the CV curves of MC-MSC, MCM-MSC, and MCMC-MSC reveal quasi-rectangular, which indicates the occurrence of electrode/electrolyte charge transfer. This charge transfer could arise from pseudocapacitive reaction if it is reversible.^[25] Meanwhile, after 10 000 cycles CV scans at 1 V s⁻¹, the MCMC-MSC maintains 96.6% of the initial capacitance; the small drop of 3.4% in capacitance is lower than many reported MSCs (the MPMP-MSC maintains 97.7% of the initial capacitance, Figure 3d). Furthermore, this cycling stability demonstrates that the electrode/electrolyte charge transfer mentioned above is reversible, and pseudocapacitive reaction occurred on the electrodes.^[25,26] From 5 to 100 mV s⁻¹, MC-MSC, MCM-MSC, and MCMC-MSC demonstrate good charge propagation across the microelectrodes (Figure S5a–c, Supporting Information).^[27] At a low scan rate, MCM-MSC exhibits a more deviation from the rectangular than that of MC-MSC, caused by more M-layer that contributed to the electrochemical reaction, as shown in Figure 3a. At a high scan rate of 500 mV s⁻¹ (Figure S5d, Supporting Information), MCMC-MSC also has a larger integral area and higher discharge current (Figure S5e, Supporting Information) than those of MC-MSC and MCM-MSC. A better linear dependence of plot of discharge current as a function of the scan rate for MCMC-MSC indicates its superior power ability.^[28] The MCMC-MSC has a larger capacitive response than those of MC-MSC and MCM-MSC at the scan rate ranging from 5 to 500 mV s⁻¹, which indicates that the strategy sufficiently improves the capacitance by increasing the loading of active materials per unit area.^[29] For monolayer MSCs, compared with C-MSC, the CV curves of M-MSC exhibit a larger rectangle, indicating a higher capacitance of M-MSC

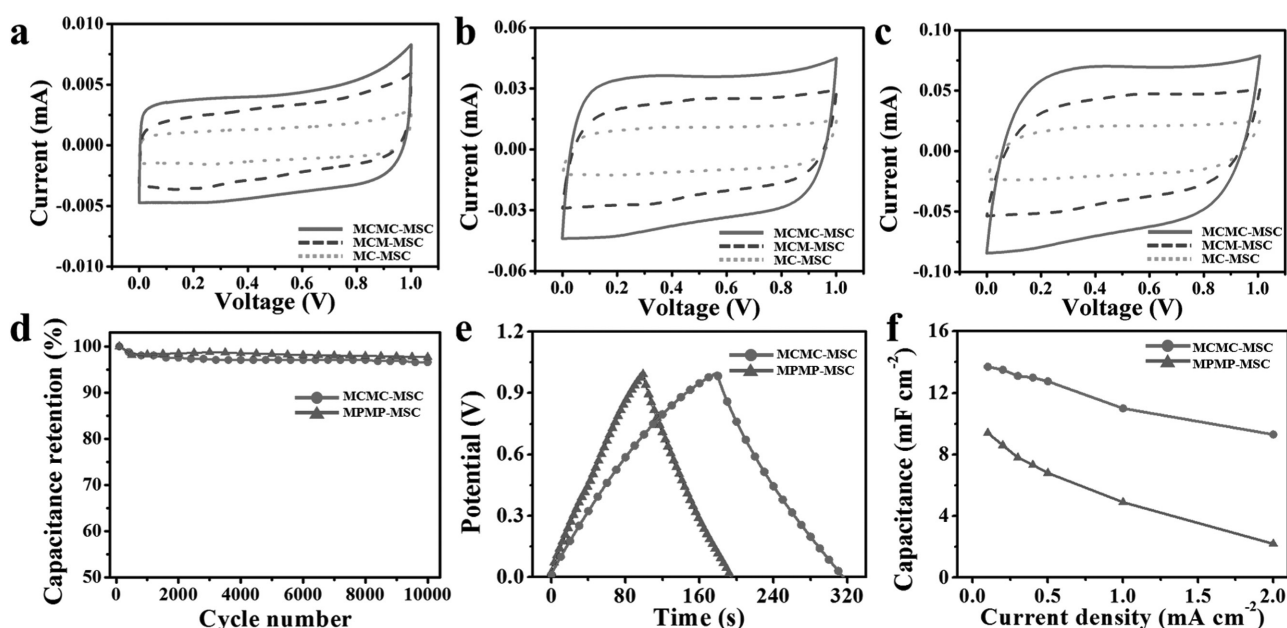


Figure 3. Electrochemical performance of MSCs. CV curves of MC-MSC, MCM-MSC, and MCMC-MSC obtained at different scan rates of a) 5, b) 50, and c) 100 mV s⁻¹. d) The capacitance retention of MCMC-MSC and MPMP-MSC at the scan rate of 1 V s⁻¹, for 10 000 cycles. e) Plots of GCD at a current density of 0.1 mA cm⁻² for MPMP-MSC and MCMC-MSC. f) Rate capabilities of MCMC-MSC and MPMP-MSC measured from GCD at different current densities.

(Figure S6a, Supporting Information). Figure S6b (Supporting Information) shows the electrochemical impedance spectroscopy (EIS) curves of the M-MSC and C-MSC. At a high frequency region, the first intercept at the real axis reflects the equivalent series resistance (R_{ES}), and the diameter of the semicircle represents the charge transfer resistance (R_{CT}).^[30] C-MSC delivers a lower R_{ES} and R_{CT} than those of M-MSC that benefited from high electrical conductivity of the MWCNTs. These phenomena demonstrate that the C-layer could effectively improve the electrical conductivity,^[28] and the capacitance of the MCMC-MSC could be significantly enhanced by M-layer.

GCD measurement is regarded as the most versatile and accurate approach in characterizing supercapacitors.^[31] To further understand the capacitance features, GCD curves of MSCs are recorded at a constant current density of 0.1 mA cm^{-2} (Figure 3e). The voltage–time response curve of MCMC-MSC during charging/discharging shows symmetric GCD profiles with a long duration time and small IR drop. The areal capacitance value depending on the current density of 0.1 mA cm^{-2} is calculated to be 13.7 mF cm^{-2} (40 F cm^{-3}). As the most widely accepted method, R_{ES} is evaluated through the analysis of the IR drop, and the value is 170Ω at a current density of 0.1 mA cm^{-2} . This relatively high R_{ES} influenced by the current collector-free structure and small width and thickness of the microelectrodes has been reported in previous studies.^[32,33] Figure S5f (Supporting Information) exhibits a variety of specific currents and the curves of the MCMC-MSC. The quasi-linear discharge curves are observed for all tested currents that also indicate the pseudocapacitance contribution of MoS_2 .^[34] However, the MPMP-MSC delivers an areal capacitance of 9.7 mF cm^{-2} , which is less than that of MCMC-MSC. The smaller capacitance of MPMP-MSC is caused by the lower capacitance contribution of the photoresist-derived carbon layers. Meanwhile, the R_{ES} increases to 302Ω at a current density of 0.1 mA cm^{-2} , indicating that the electrical conductivity of the MCMC-MSC is observably enhanced by MWCNTs. The enhancement of the electrical conductivity of the MSC is essential in improving the power performance and energy efficiency.^[31,35] The areal capacitances of MCMC-MSC and MPMP-MSC as a function of current density are compared in Figure 3f. Gradually increased discharge current results in the drop of capacitance. The capacitance retention of MCMC-MSC and MPMP-MSC is 68% and 23%, respectively, with the current density ranging from 0.1 to 2 mA cm^{-2} (0.3 to 5.9 A cm^{-3}) in the potential window of 0 – 1 V . This superiority is dramatically more pronounced at a higher scan rate for MCMC-MSC. Therefore, the MCMC-MSC can achieve much higher power density.^[33]

EIS is used to confirm the ion transport property. As shown in Figure 4, at low frequency, large slopes with tendency toward vertical line are obtained for MCMC-MSC and MPMP-MSC where the imaginary part of impedance rapidly increases, indicating an approximately ideal capacitive behavior with highly accessible surface of the pores on the surface.^[36,37] At high frequency region, high R_{CT} of MPMP-MSC is considered to be affected by porous geometries due to the high resistance to ionic transport in small pores.^[25,38,39] MCMC-MSC exhibits a smaller R_{CT} than MPMP-MSC,

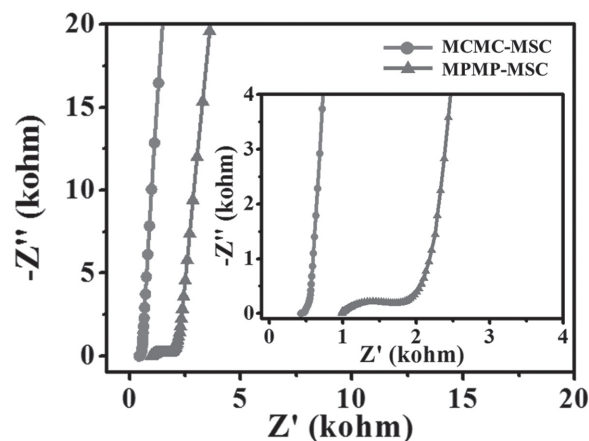


Figure 4. Nyquist plots of MCMC-MSC and MPMP-MSC with a magnification of the high-frequency region (inset).

which benefited from partial interface separation in C-layers that provides more gaps and electrode/electrolyte interfaces. These gaps offer more pathways for ion transport and achieve rapid ion transport in the electrodes. Meanwhile, the increased electrode/electrolyte interfaces around CNTs lead to more pathways for electron transport. The synergistic effect of the enhanced ion transport and electron transport will result in lower resistance of MCMC-MSC, which is quite crucial important since less energy and power will be wasted during charge and discharge processes.

Energy density and power density are critical parameters in evaluation of energy storage device practicability. The MCMC-MSC delivers a high energy density of 5.6 mWh cm^{-3} ($1.9 \mu\text{Wh cm}^{-2}$) at a current density of 0.1 mA cm^{-2} , which exceeds most reported carbon-based MSCs, about 1.6 mWh cm^{-3} for onion-like carbon MSC,^[40] 3 mWh cm^{-3} for photoresist-derived carbon MSC,^[25] 4.0 mWh cm^{-3} for laser-writing graphite MSC,^[41] and MoS_2 -based MSC, about 0.58 mWh cm^{-3} for MSC by gravure printing.^[11] Figure 5a,b shows the Ragone plot of the specific energy versus power density of MCM-MSC. The volumetric energy density of MCMC-MSC (at the current density of 0.1 mA cm^{-2}) is higher than that of reported MSCs, such as MWCNT/carbon MSC,^[18] LSG/SWCNTs MSC,^[42] and MnO_x/Au MSC.^[33] Neither thin film lithium-ion batteries nor conventional supercapacitors can provide the high energy and power density as the proposed alternating stacked MCMC-MSC.^[40] It is notable that the areal energy density of MCMC-MSC is one order higher than those reported MSCs. The high areal energy density and power density of MCMC-MSC mainly contributed from the high pseudocapacitive properties of MoS_2 and the narrow gaps between microelectrodes by this fully controlled micropatterning. The alternating stacked structures could improve mass loading of active materials in limited footprint area, and enhance the electrical conductivity of MSC.

3. Conclusion

In summary, we report a novel microfabrication process of all-solid-state MSCs with alternating stacked M- and C-layers

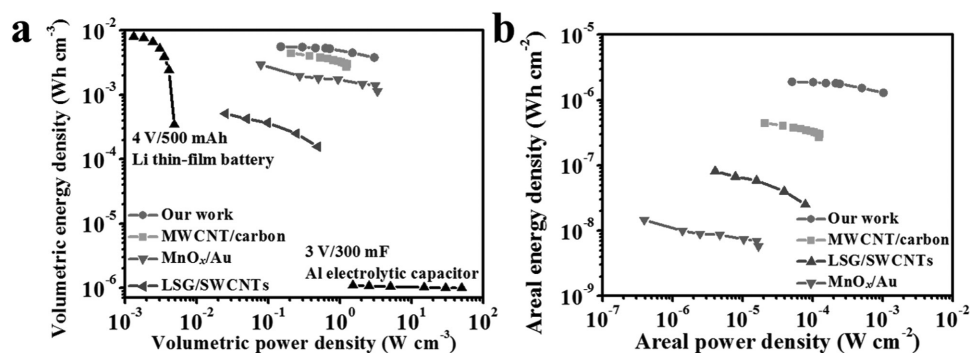


Figure 5. Comparison in Ragone plots, of a) volumetric and b) areal specific energy density and power density of MCMC-MSC with MWCNT/carbon MSC, LSG/SWCNT MSC, and MnO_x/Au MSC.

by optimized micropatterning and pyrolysis. MWCNTs effectively improve the electrical conductivity of the whole MSC, and the M-layer mostly attributes to the capacitance of the MSC. The gaps, resulting from interface separation, pose a positive effect on the ion diffusion and further enhance the performance of the MCMC-MSC. The MCMC-MSC has a high energy density, good capacitance retention rate, and outstanding cycling performance. The proposed micro-fabrication process is highly promising in fabrication of high-performance MSCs, ion capacitors, and microbatteries, which is very important and highly attractive for various application fields.

4. Experimental Section

Synthesis of MoS_2 Nanosheets@rGO: The MoS_2 nanosheets@rGO were synthesized via a conventional one-step hydrothermal method.^[19] 0.8 g $\text{Na}_2\text{MoO}_4 \cdot 2\text{H}_2\text{O}$ was dispersed in 30 mL deionized (DI) water by vigorous stirring. Then 6 mg rGO powders (XF NANO, Inc. Co., Ltd.) were dissolved in the above solution. After ultrasonication for 1 h, 1.26 g NH_2CSNH_2 was dissolved in the solution. Followed by 2 h ultrasonication, the solution was transferred into a 50 mL Teflon-line stainless steel autoclave and maintained at 200 °C for 24 h. After cooling down to room temperature naturally, the black precipitate was collected by centrifugation with DI water and ethanol for several times, and then dried in a vacuum oven at 70 °C for 12 h.

Microfabrication of Alternating Stacked MoS_2 @rGO-CNT MSCs: For the microfabrication process of MSCs, first, 0.15 g MoS_2 @rGO was mixed with 1.35 g PR1-9000A photoresist and 15 drops of SD1 diluent (Futurrex, Inc. Co., Ltd.), followed by stirring and ultrasonic agitation for 12 h at room temperature. Afterward, a uniform M-photoresist was obtained. C-photoresist was prepared by mixing 0.01 g MWCNT (XF NANO, Inc. Co., Ltd.), 0.99 g PR1-9000A photoresist, and 5 drops of SD1 diluent, followed by the same procedure as M-photoresist. After standing for 1 h, the C-photoresist and M-photoresist were successively spin coated on RCA cleaned Si/SiO₂ substrate by 1000 revolution per minute (rpm) for 10 s and 6000 rpm for 40 s. Then the spin coating was repeated twice to obtain the MCMC-film. Parameters of spin coating and content of SD1 diluent were optimized to achieve uniform composite films with smooth surface. Afterward, 18 min soft baking of the films at 100 °C in the drying oven was conducted.

The interdigital micropattern with 14 in-plane fingers (the pattern of mask has seven fingers per polarity, each finger has a size of 2800 × 120 μm, and the gap distance of each fingers is 60 μm) is shown in Figure S7 (Supporting Information), which was achieved from MCMC-film using optimized photolithography with a dose of 1440 mJ cm⁻², and development of 150 s in RD6 developer (Futurrex, Inc. Co., Ltd.). Optical microscope images demonstrated that the MoS_2 @rGO were well distributed in the photoresist (Figure S8a, Supporting Information). Then the interdigital micro-electrodes were fabricated by pyrolyzing the prepared micropattern in N₂ flow. During the pyrolysis, the temperature of furnace increased to 400 °C by 2 °C min⁻¹, and held at this temperature for 30 min, then increased to 900 °C at a rate of 2 °C min⁻¹, and kept at this temperature for 1 h, and finally the furnace was cooled down to room temperature naturally. After annealing, the photoresist shrank drastically and MoS_2 @rGO had a dense distribution on the surface (Figure S8b, Supporting Information). The content of MoS_2 @rGO in M-layer was about 61.7 wt% and the content of MWCNT in C-layer was about 6.2%, calculated from weight loss of photoresist during annealing.^[14] The gel electrolyte was prepared by mixing 5 g PVA and 5 g H₂SO₄ into 50 mL DI water, and heated at 80 °C until the solution became clear. Afterward, H₂SO₄/PVA was employed as the electrolyte of MSCs.

Materials and Devices Characterization: The SEM images were collected with a JEOL JSM-7100F SEM at an acceleration voltage of 20 kV. The TEM images were acquired using a Titan G2 60-300 Probe Cs Corrector high resolution scanning TEM (HRSTEM). The XRD characterization was conducted by D8 DISCOVER X-ray diffractometer, using Cu Kα radiation ($\lambda = 1.5418 \text{ \AA}$). The thicknesses of the microelectrodes were measured by stylus surface profiler (Bruker DEKTAK XT).

Electrochemical Characterization: The electrochemical performance of the MSCs was examined by conducting CV tests, GCD tests, and EIS tests using an Autolab 302N. Both CV and GCD tests were conducted using a two-electrode system, while the EIS tests adopted the frequency ranging from 0.01 Hz to 500 kHz at an open-circuit potential with an AC perturbation of 10 mV.

The areal capacitance of MCMC-MSC was calculated by using the following equation:^[32]

$$C_{\text{area}} = \frac{I \Delta t}{A \Delta V} \quad (1)$$

where C_{area} is the areal specific capacitance, I is the current, Δt is the discharge time after IR drop, ΔV is the potential window, and A

is the area of the microelectrodes. The microelectrodes area of the MCMC-MSC is 0.0618 cm², as shown in Figure S6 (Supporting Information).

The R_{ES} was evaluated through the analysis of the IR drop, and the calculation equation is as follows:^[31]

$$R_{ES} = \frac{\Delta V}{\Delta I} \quad (2)$$

The ΔV and ΔI are the voltage and current of the IR drop, respectively.

The volumetric energy density (E_v), volumetric power density (P_v), areal energy density (E_a), and areal power density (P_a) were calculated using the following equations:^[43]

$$E_v = \frac{C_{area}V^2}{7200t} \quad (3)$$

$$P_v = \frac{E_v}{\Delta t} \times 3600 \quad (4)$$

$$E_a = \frac{C_{area}V^2}{7200} \quad (5)$$

$$P_a = \frac{E_a}{\Delta t} \times 3600 \quad (6)$$

where E is the energy density, P is the power density, C_{area} is the areal specific capacitance calculated through GCDs, V is the voltage window width, t is the thickness of microelectrodes, and Δt is the discharge time.

Supporting Information

Supporting Information is available from the Wiley Online Library or from the author.

Acknowledgements

This work was supported by the National Key Research and Development Program of China (2016YFA0202603 and 2016YFA0202604), the National Basic Research Program of China (2013CB934103), the Programme of Introducing Talents of Discipline to Universities (B17034), the National Natural Science Foundation of China (51521001, 51502227, and 51579198), the China Postdoctoral Science Foundation (2015T80845), the Hubei Province Natural Science Fund (2016CFB582), and the Fundamental Research Funds for the Central Universities (WUT: 2016III001 and 2016III005). L.H. and L.Q.M. gratefully acknowledge financial support from the China Scholarship Council (Grant Nos. 201606955094 and 201606955096).

Conflict of Interest

The authors declare no conflict of interest.

- [1] M. Beidaghi, Y. Gogotsi, *Energy Environ. Sci.* **2014**, *7*, 867.
- [2] N. A. Kyremateng, T. Brousse, D. Pech, *Nat. Nanotechnol.* **2017**, *12*, 7.
- [3] A. Ferris, S. Garbarino, D. Guay, D. Pech, *Adv. Mater.* **2015**, *27*, 6625.
- [4] L. L. Zhang, X. S. Zhao, *Chem. Soc. Rev.* **2009**, *38*, 2520.
- [5] X. Tian, M. Shi, X. Xu, M. Yan, L. Xu, A. Minhas-Khan, C. Han, L. He, L. Mai, *Adv. Mater.* **2015**, *27*, 7476.
- [6] K. Chang, W. Chen, *ACS Nano* **2011**, *5*, 4720.
- [7] E. G. da Silveira Firmiano, A. C. Rabelo, C. J. Dalmaschio, A. N. Pinheiro, E. C. Pereira, W. H. Schreiner, E. R. Leite, *Adv. Energy Mater.* **2014**, *4*, 1301380.
- [8] X. Hu, W. Zhang, X. Liu, Y. Mei, Y. Huang, *Chem. Soc. Rev.* **2015**, *44*, 2376.
- [9] Z. S. Wu, K. Parvez, X. Feng, K. Müllen, *Nat. Commun.* **2013**, *4*, 2487.
- [10] H. Wang, H. Feng, J. Li, *Small* **2014**, *10*, 2165.
- [11] Y. Xiao, L. Huang, Q. Zhang, S. Xu, Q. Chen, W. Shi, *Appl. Phys. Lett.* **2015**, *107*, 013906.
- [12] L. Cao, S. Yang, W. Gao, Z. Liu, Y. Gong, L. Ma, G. Shi, S. Lei, Y. Zhang, S. Zhang, R. Vajtai, P. M. Ajayan, *Small* **2013**, *9*, 2905.
- [13] M. Beidaghi, W. Chen, C. Wang, *J. Power Sources* **2011**, *196*, 2403.
- [14] C. Yin, L. He, Y. Wang, Z. Liu, G. Zhang, K. Zhao, C. Tang, M. Yan, Y. Han, L. Mai, *RSC Adv.* **2016**, *6*, 43436.
- [15] M. Beidaghi, C. Wang, *Electrochim. Acta* **2011**, *56*, 9508.
- [16] W. Zhang, S. Zhu, R. Luque, S. Han, L. Hu, G. Xu, *Chem. Soc. Rev.* **2016**, *45*, 715.
- [17] R. L. McCreery, *Chem. Rev.* **2008**, *108*, 2646.
- [18] Y. Yang, L. He, C. Tang, P. Hu, X. Hong, M. Yan, Y. Dong, X. Tian, Q. Wei, L. Mai, *Nano Res.* **2016**, *9*, 2510.
- [19] F. Li, L. Zhang, J. Li, X. Lin, X. Li, Y. Fang, J. Huang, W. Li, M. Tian, J. Jin, R. Li, *J. Power Sources* **2015**, *292*, 15.
- [20] Y. J. Tang, Y. Wang, X. L. Wang, S. L. Li, W. Huang, L. Z. Dong, C. H. Liu, Y. F. Li, Y. Q. Lan, *Adv. Energy Mater.* **2016**, *6*, 1600116.
- [21] Z. Hu, L. Wang, K. Zhang, J. Wang, F. Cheng, Z. Tao, J. Chen, *Angew. Chem. Int. Ed.* **2014**, *53*, 12794.
- [22] Y. Liu, L. Jiao, Q. Wu, Y. Zhao, K. Cao, H. Liu, Y. Wang, H. Yuan, *Nanoscale* **2013**, *5*, 9562.
- [23] B. Hsia, M. S. Kim, M. Vincent, C. Carraro, R. Maboudian, *Carbon* **2013**, *57*, 395.
- [24] J. Lin, C. Zhang, Z. Yan, Y. Zhu, Z. Peng, R. H. Hauge, D. Natelson, J. M. Tour, *Nano Lett.* **2013**, *13*, 72.
- [25] S. Wang, B. Hsia, C. Carraro, R. Maboudian, *J. Mater. Chem. A* **2014**, *2*, 7997.
- [26] B. E. Conway, V. Birss, J. Wojtowicz, *J. Power Sources* **1997**, *66*, 1.
- [27] Z. S. Wu, K. Parvez, A. Winter, H. Vieker, X. Liu, S. Han, A. Turchanin, X. Feng, K. Müllen, *Adv. Mater.* **2014**, *26*, 4552.
- [28] R. Z. Li, R. Peng, K. D. Kihm, S. Bai, D. Bridges, U. Tumuluri, Z. Wu, T. Zhang, G. Compagnini, Z. Feng, A. Hu, *Energy Environ. Sci.* **2016**, *9*, 1458.
- [29] J. Chmiola, C. Largeot, P. L. Taberna, P. Simon, Y. Gogotsi, *Science* **2010**, *328*, 480.
- [30] Z. Su, C. Yang, B. Xie, Z. Lin, Z. Zhang, J. Liu, B. Li, F. Kang, C. P. Wong, *Energy Environ. Sci.* **2014**, *7*, 2652.
- [31] S. Zhang, N. Pan, *Adv. Energy Mater.* **2015**, *5*, 1401401.
- [32] X. Wang, B. D. Myers, J. Yan, G. Shekhawat, V. Dravid, P. S. Lee, *Nanoscale* **2013**, *5*, 4119.
- [33] W. Si, C. Yan, Y. Chen, S. Oswald, L. Han, O. G. Schmidt, *Energy Environ. Sci.* **2013**, *6*, 3218.
- [34] B. Hsia, M. S. Kim, C. Carraro, R. Maboudian, *J. Mater. Chem. A* **2013**, *1*, 10518.
- [35] L. G. H. Staaf, P. Lundgren, P. Enoksson, *Nano Energy* **2014**, *9*, 128.
- [36] Z. S. Wu, K. Parvez, S. Li, S. Yang, Z. Liu, S. Liu, X. Feng, K. Müllen, *Adv. Mater.* **2015**, *27*, 4054.
- [37] G. Lee, D. Kim, D. Kim, S. Oh, J. Yun, J. Kim, S. S. Lee, J. S. Ha, *Energy Environ. Sci.* **2015**, *8*, 1764.

- [38] J. Chang, S. Adhikari, T. H. Lee, B. Li, F. Yao, D. T. Pham, V. T. Le, Y. H. Lee, *Adv. Energy Mater.* **2015**, *5*, 1500003.
- [39] C. Hitz, A. Lasia, *J. Electroanal. Chem.* **2001**, *500*, 213.
- [40] D. Pech, M. Brunet, H. Durou, P. Huang, V. Mochalin, Y. Gogotsi, P. L. Taberna, P. Simon, *Nat. Nanotechnol.* **2010**, *5*, 651.
- [41] W. Gao, N. Singh, L. Song, Z. Liu, A. L. M. Reddy, L. Ci, R. Vajtai, Q. Zhang, B. Wei, P. M. Ajayan, *Nat. Nanotechnol.* **2011**, *6*, 496.
- [42] F. Wen, C. Hao, J. Xiang, L. Wang, H. Hou, Z. Su, W. Hu, Z. Liu, *Carbon* **2014**, *75*, 236.
- [43] X. Tian, B. Xiao, X. Xu, L. Xu, Z. Liu, Z. Wang, M. Yan, Q. Wei, L. Mai, *Nano Res.* **2016**, *9*, 1012.

Received: February 26, 2017
Revised: March 20, 2017
Published online: